I&EC research
Industrial & Engineering Chemistry Research
pubs.acs.org/IECR
Article

Coupling Covalent Organic Frameworks and Carbon Nanotube Membranes to Design Easily Reusable Photocatalysts for Dye Degradation

Hongbo Xue, Zhijie Bi, Jiayu Cheng, Sen Xiong,* and Yong Wang*

Cite This: *Ind. Eng. Chem. Res.* 2021, 60, 8687−8695
Read Online

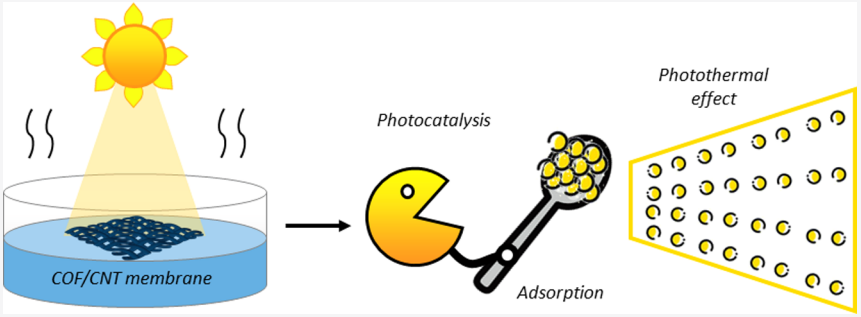

ABSTRACT: Covalent organic frameworks (COFs) have been used as photocatalysts, but recovering COF particulates from aquatic environments is tedious and labor-consuming. In order to maximize the photocatalytic performance and simplify the degradation processes, carbon nanotube (CNT) membranes with excellent electron transfer capacity and photothermal effects are used as substrates to fabricate COF/CNT membranes. The uniform COF layer enhances the mechanical property and hydrophilicity of the CNT membranes. Meanwhile, by utilizing the large surface area and photothermal effect of the CNT membranes, the photocatalytic activity of COF-based composite membranes can be improved to match that of pure COF particulates. Due to the positive interaction between COFs and CNT membranes, the composite membranes exhibit superior degradation capacity toward mordant black 17 (MB17) with strong handleability. The total degradation capacity of COF/CNT membranes can reach 708.2 mg/g, and the composite membranes can be reused seven times with only 10.6% efficiency loss in degradation capacity.

1. INTRODUCTION

There are more than 10,000 types of dyes used in industry, and the annual output of synthetic dyes exceeds 700,000 tons.[1−3] Among them, the most frequently and massively used are azo dyes, which account for more than 60% of the total output.[4,5] During the production and usage, a large amount of dye-containing wastewater is generated and discharged without appropriate treatments. Dyes can accumulate in organisms easily, and most of them are carcinogenic, mutagenic, or teratogenic to both animals and humans.[6] Therefore, dye-containing wastewater has become a huge hidden danger to human health.[7] Dyes are stable in natural water systems, and traditional water purification treatments exhibit low treatment efficiency.[8] Flocculation is the simplest and most economical method, but the harmful by-products will cause secondary pollution.[6] Although adsorption is highly efficient without harmful by-products, the expensive regeneration cost of the adsorbent and the intractable residual pollutants impede it from actual uses.[9,10] Electrochemical treatment method has many merits such as simple operation, fast dealing speed, and high efficiency, but the huge energy consumption limits its large scale utilization.[2]

As an advanced oxidation technology, photocatalysis shows many distinctive features, such as ultralow energy consumption, simple operation, and nonpollution, and its potential has been demonstrated in many fields including hydrogen production, carbon dioxide reduction, organic synthesis, and so on.[11,12] Many emerging materials such as metal organic frameworks (MOFs) and carbon nitride (C_3N_4), as well as traditional metal oxides, have been investigated in photocatalysis.[13−17] However, there are still some urgent problems, such as light corrosion, low photocatalytic efficiency, poor reusability, and applicability, need to be solved.[18,19]

Covalent organic frameworks (COFs) are a kind of porous organic crystalline materials that organize structural units through strong covalent bonds.[20,21] The $\pi-\pi$-stacked two-

Received: March 31, 2021
Revised: May 31, 2021
Accepted: June 1, 2021
Published: June 10, 2021

https://doi.org/10.1021/acs.iecr.1c01254
Ind. Eng. Chem. Res. 2021, 60, 8687−8695

Scheme 1. Diagram of the COF/CNT Membrane Synthesis and the Photocatalytic Degradation Process

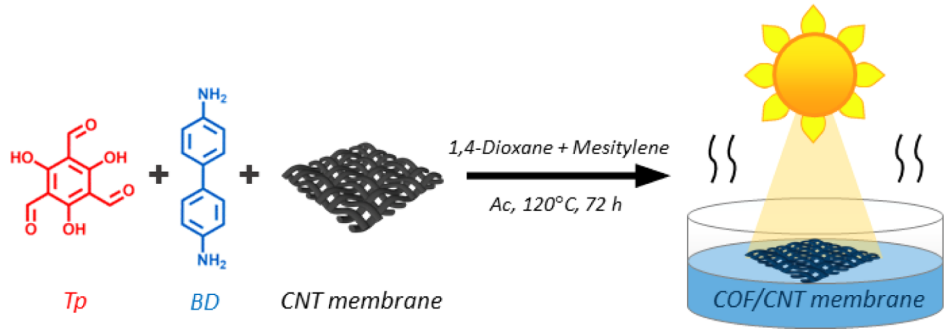

dimensional structure promotes the migration of photoelectrons from holes, and improves the efficiency and lifetime of photoelectrons.[22,23] The appropriate energy band structure makes COFs absorb a wider range of light, which leads to a better use of natural light.[24] The porous structure of COFs can adsorb pollutants effectively, and provide more active sites when used as catalysts.[25] COFs are completely composed of light elements without any metal elements. Therefore, the metal ion pollution caused by the light corrosion can be avoided.[26] By choosing different structural units, COFs can be designed and synthesized according to the requirements of various photocatalytic systems.[21] Moreover, excellent thermal and chemical stabilities of COFs ensure serviceability under various extreme conditions.[21] Due to these merits, COFs have been explored in photocatalysis for many applications, such as photocatalytic hydrogen production,[27] CO_2 redox reaction,[28] cis−trans isomerization of olefins,[29] bacteria inactivation,[30] and degradation of organic pollutants.[31] Although COFs exhibit enhanced catalytic efficiency in the form of particulates, they are hard to recover from the treating system, especially in the aquatic environments. Therefore, an easy-to-operate method for COF-based photocatalysis applied in wastewater treatments is required.

Carbon nanotubes (CNTs) are a typical type of one-dimensional materials with nanoscale diameters and microscale lengths.[32] Because of their excellent electrical conductivity, CNTs are commonly used as a Z-scheme heterojunction medium in the photocatalytic process.[33] Meanwhile, CNTs exhibit an excellent photothermal effect, which may increase the temperature of the treating system and provide extra energy for photocatalysis. The photothermal effect can accelerate water evaporation and concentrate the solution system, which will further enhance photocatalytic efficiency.[34] CNTs with a high aspect ratio tend to interweave to form porous membranes. CNT membranes can be modified or combined with other materials by solvothermal methods thanks to the decent chemical and thermal stability.[35] As a result, CNT membranes have been applied as substrates or electron transfer media for photocatalysis, such as photocatalytic hydrogen production,[36] degradation of dyes,[37] and decomposition of ciprofloxacin.[34] However, the strong hydrophobicity of CNT membranes limits their applications in aquatic milieu.

In our previous work, a commonly used COF, TpBD, was demonstrated to be an outstanding photocatalyst with wide natural light absorption ranges.[38] In order to make the best use of TpBD, in the present work we directly grew it on the CNT membranes to fabricate COF/CNT membranes with better usability. The strong hydrophobic surface of the CNT membranes was substituted by the hydrophilic TpBD, which enhanced the affinity between photocatalytic membranes and water. Multiwalled CNT membranes were taken as substrates due to abundant surface active groups, which can be firmly attached by COFs. The TpBD was uniformly integrated into the membrane skeleton, ensuring large accessible surface areas for pollutant adsorption, light absorption, and photodegradation. Moreover, the photothermal effect of the CNT membranes accelerated the photodegradation processes, while the uniform COF layer enhanced the mechanical property of the CNT membranes. Through this simple coupling strategy, a high-performance membrane-type photocatalyst is fabricated, which expands applications of both COFs and CNTs in photocatalysis and opens a new avenue to produce more practicable photocatalysts.

2. EXPERIMENTAL SECTION

2.1. Materials. The multiwalled CNT (Suzhou Jiedi Nanotechnology Co., Ltd.) membranes were employed as substrates. 2,4,6-Triformylphloroglucinol (Tp, 98%, Yanshen Technology Co., Ltd.) and benzidine (BD, 95%, Aladdin) were used as monomers. Mordant black 17 (MB17, Macklin) was employed as the model pollutant. Ethylenediaminetetraacetic acid disodium salt (EDTA-2Na, 99.95%, Institute of Chemical Reagent), *p*-benzoquinone (BQ, 98%, Hushi), and *tert*-butanol (*t*-BuOH, 98%, Aladdin) were used as scavengers. Fluoride tin oxide (FTO, Crystalgen Ningbo Biotech Ltd.) conducting glass, Nafion 117 (5%, Sigma-Aldrich), and Na_2SO_4 (99%, Aladdin) were used during electrochemical tests. 1,3,5-Trimethylbenzene (97%), 1,4-dioxane (99%), ethanol (99.8%), acetic acid (Ac, 99%), and deionized water were purchased from local suppliers. All reagents were used as received.

2.2. Synthesis of COF/CNT Membranes. COF/CNT membranes were solvothermally synthesized. Different moles (0.3, 0.5, and 1 mmol) of Tp and the corresponding moles of BD (0.45, 0.75, and 1.5 mmol) were employed as monomers. 30 mL 1,4-dioxane, 30 mL mesitylene, and 0.5 mL acetic acid (18 M) were added into a Teflon-lined reactor (100 mL) in sequence and then ultrasonically treated for 20 min to ensure homogeneous dispersion of the mixture. Afterward, two pieces of CNT membranes (50 mm × 50 mm) were added into the reactor (to perform the reaction at 120 °C) for 72 h. Then, the membranes were taken out and washed with ethanol. To completely remove COF particulates precipitated on the membrane surfaces, 15 s ultrasonic treatment was applied. Finally, the obtained COF/CNT membranes were dried at 120 °C for 2 h (Scheme 1). According to the concentration of monomer Tp (0.3, 0.5 and 1 mmol), photocatalytic membrane

https://doi.org/10.1021/acs.iecr.1c01254
Ind. Eng. Chem. Res. 2021, 60, 8687−8695

samples were named COF/CNT membrane-0.3, -0.5, and -1, respectively. All CNT membranes and COF/CNT membranes were weighed before synthesis and after drying to record the mass changes.

2.3. Characterization. Morphologies of COF/CNT membranes were characterized using a field-emission scanning electron microscope (Hitachi S-4800) at an accelerating voltage of 5 kV. Prior to the test, a thin layer of gold was sputter-coated onto samples to enhance conductivity. Fourier transform infrared (FTIR, Nicolet 8700, Thermo Fisher Scientific) spectroscopy was used to analyze the chemical composition of monomers, COFs particulates, and COF/CNT membranes. Monomers and COF particulates were mixed with the potassium bromide and pressed into disks for FTIR tests. COF/CNT membranes were tested by the attenuated total reflectance (ATR) method using original CNT membranes as background. Powder X-ray diffraction (PXRD, Rigaku SmartLab) was used to analyze the crystallinity of COFs. The measurements were conducted at room temperature with 2θ ranging from 0.5 to 30° and at a scanning rate of 0.02°/s.

The hydrophilicity of membranes was analyzed by testing their water contact angles with a goniometer (WCA, DropMeter A100, Maist), and the average value was obtained by testing at least three positions for each samples. A universal testing instrument (ETM105D-TS, Wance) was employed to test mechanical properties of membranes. All the samples were cut into strips (10 mm × 100 mm), and the testing length was 35 mm. An UV−visible−near-infrared diffuse reflectance spectrophotometer (Shimazu UV-3600) was used in the wavelength from 300 to 700 nm to analyze the energy gaps and absorbance edges of catalysts. Electrochemical property of TpBD was characterized by an electrochemical workstation (CHI660E, Shanghai Chenhua). 0.5 mg TpBD particulates were dispersed in 1 mL ethanol with 50 μL Nafion 117 and then ultrasonicated for 20 min. 100 μL of the mixture was dropped on the surface of FTO conducting glass (10 mm × 30 mm) and dried at room temperature. During the test, TpBD-coated FTO conducting glass was used as the working electrode, Pt was used as the counter electrode, and Ag/AgCl was used as the reference electrode. Conducting bands were tested by the Mott−Schottky (M−S) analysis with 30 mL Na_2SO_4 (0.5 M, pH = 7) as the electrolyte.

2.4. Photocatalytic Tests. The process of adsorption was dynamically equilibrious,[39] thus the adsorption of photocatalysts was variable with the concentration of solutions. To accurately calculate the degradation of adsorbed dyes by COF/CNT membranes, the equilibrium adsorption curve of MB17 was essential. A piece of COF/CNT membrane (50 mm × 50 mm) was immersed in 200 mL MB17 solutions with different concentrations (20−120 mg/L), and stirred at 200 rpm for 12 h in the dark to reach adsorption equilibrium. The equilibrium adsorption capacity of COF/CNT membranes was determined by comparing the dye concentration before and after adsorption. Finally, the relationship between adsorption capacities and solution concentrations was drawn as the equilibrium adsorption curve. UV−visible absorption (UV−vis, NanoDrop 2000c, Thermo Fisher Scientific) spectroscopy was employed to determine the absorbance of dye solutions. Equilibrium adsorption capacity of membranes was calculated using eq 1

$$q = \frac{V \times \frac{(A_0 - A_e)}{A_0} \times C_0}{m} \quad (1)$$

where q represents the adsorption capacity (mg/g), V is the volume of the solution (mL), and A_0 and A_e are the original and equilibrium absorbance of the solutions, respectively. C_0 is the original concentration (mg/L) and m is the mass of catalysts (g).

Two pieces of membranes (50 mm × 50 mm) were stirred at 200 rpm in 1 L MB17 solution (115 mg/L) in the dark for 12 h to reach adsorption equilibrium and then tested the absorbance. 50 mL MB17 solution (100 mg/L) and one piece of the saturated membrane were added into a glass vessel (60 mm in diameter and 30 mm in height) with 200 rpm stirring under the irradiation of a 300 W Xenon lamp (100 mW/cm^2, Perfect Light, PLS-SXE 300). Samples were taken out and tested every 30 min, and then put back into the vessel after the UV−vis test. Due to the large adsorption capacity of COF/CNT membranes, the adsorbed dyes should not be neglected. Dyes from solutions and adsorptions were both considered in eqs 2−4

$$D = D_m + D_s \quad (2)$$

$$D_m = q_0 - q_t \quad (3)$$

$$D_s = \frac{V \times \frac{A_0 - A_t}{A_0} \times C_0}{m} \quad (4)$$

where D_m, D_s, and D represent the degradation of dyes in membranes, solutions, and the total degradation amount (mg/g). q_0 and q_t are the original and instant adsorption capacities of the membranes (mg/g) calculated from the equilibrium adsorption curve, respectively. V is the volume of the solution (mL), and A_0 and A_t are the original and instant absorbance of the solutions, respectively. C_0 is the original concentration (mg/L) and m is the mass of catalysts (g). The diagram of dye degradation components is shown in Scheme 2. The same

Scheme 2. Diagram of Dye Degradation Components

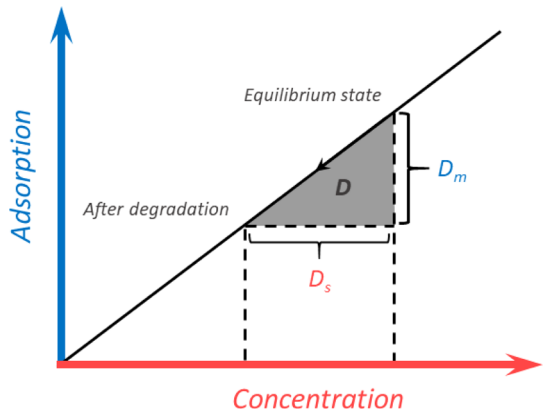

method was used in the durability test. After degradation for 3 h, the tested membranes were taken out and then directly immersed into the 1 L MB17 solution (105 mg/L) with stirring at 200 rpm for 12 h to reach adsorption equilibrium. Finally, the saturated COF/CNT membranes were reused for photocatalysis experiments. All the operations were repeated seven times.

https://doi.org/10.1021/acs.iecr.1c01254
Ind. Eng. Chem. Res. 2021, 60, 8687−8695

A contact thermocouple (52-II, Fluke) and an electronic balance were used to record the photothermal effect of COF/CNT membranes. A 300 W Xenon lamp (100 mW/cm^2) was employed as the light source at 25 °C and 40% relative humidity. 50 mL MB17 solution (100 mg/L) and CNT membranes, COF/CNT membranes, or 10 mg TpBD particulates were added into a glass vessel, and the mass and temperature changes of the solutions were recorded.

During the photocatalytic degradation, BQ, *t*-BuOH, and EDTA-2Na were used as scavengers for $^{\bullet}O_2^-$, $^{\bullet}OH$, and h^+, respectively. 1 mM scavenger was added into the solution before the test. Performances of free radicals were evaluated by changes of degradation.

3. RESULTS AND DISCUSSION

3.1. Characterization of COF/CNT Membranes. SEM was used to characterize the surface morphologies of CNT and COF/CNT membranes (Figure 1). With the addition of monomers, the COF TpBD grew along the CNTs, and the interspace of CNTs was filled up gradually. For the COF/CNT membrane-0.3, -0.5 and -1 (50 mm × 50 mm), the mass increases were 13, 15, and 18.5 mg, respectively (Table S1). When the concentration was 0.5 mmol, the COF grew uniformly along CNTs (Figure 1c). Upon further increasing the concentration to 1 mmol, excess monomers continued to grow on already saturated CNTs, filling up pores and growing into patches on the surface of the composite membrane (Figure 1d).

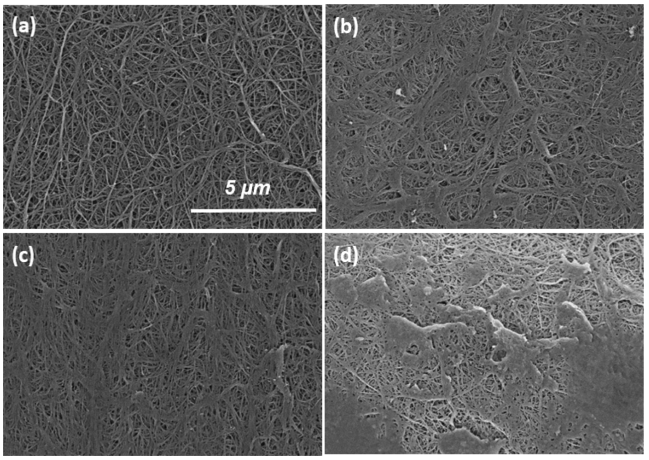

Figure 1. SEM images of (a) CNT membranes, (b) COF/CNT membrane-0.3, (c) COF/CNT membrane-0.5, and (d) COF/CNT membrane-1. All images are in the same magnification.

FTIR was used to characterize the chemical composition of the monomers, COFs particulates, and COF/CNT membranes. As shown in Figure 2a, obvious stretching vibration peaks of CH═O (2898 cm^{-1}) and C═O (1643 cm^{-1}) were presented in the spectrum of Tp while the strong stretching vibration peak of N−H (3300−3100 cm^{-1}) was shown in the spectrum of BD. After reaction, the N−H peak of BD and the CH═O peak of Tp disappeared completely, while new peaks of C═C (1597 cm^{-1}), C═C (Ar) (1450 cm^{-1}) and C−N (1258 cm^{-1}), which can be assigned to the COF product, TpBD, arose.[40] The FTIR spectrum of the COF/CNT membranes (CNT membranes as the background, ATR method) was completely consistent with the infrared spectrum of the TpBD particulates. The generation of new characteristic peaks proved that the monomers went through keto−enol tautomerism, and the TpBD was successfully grown on CNT membranes.

PXRD was used to characterize the crystal structure of TpBD particulates. Due to the high reactivity of monomers, TpBD not only grew on the CNT membranes but also generated in the solvent in particulate form. Because the amount of COF grown on the CNT membranes was fairly low, the COF particulates obtained in the same reactor were collected and used for the PXRD characterization as the substitute. As shown in Figure 2b, TpBD had an obvious characteristic peak at 3.38° (corresponding to the (100) plane), indicating that TpBD had a relatively regular and homogeneous pore structure and good crystallinity. The characteristic peak at 27.28° corresponds to the (001) crystal plane, indicating that TpBD had a regular $\pi-\pi$ stacking structure.[41] This regular and orderly parallel structure would increase the migration of photo-generated electrons, thereby enhancing the efficiency of photocatalytic degradation.[21]

3.2. Photocatalytic Degradation Performance and Mechanism. With the introduction of CNT membranes and

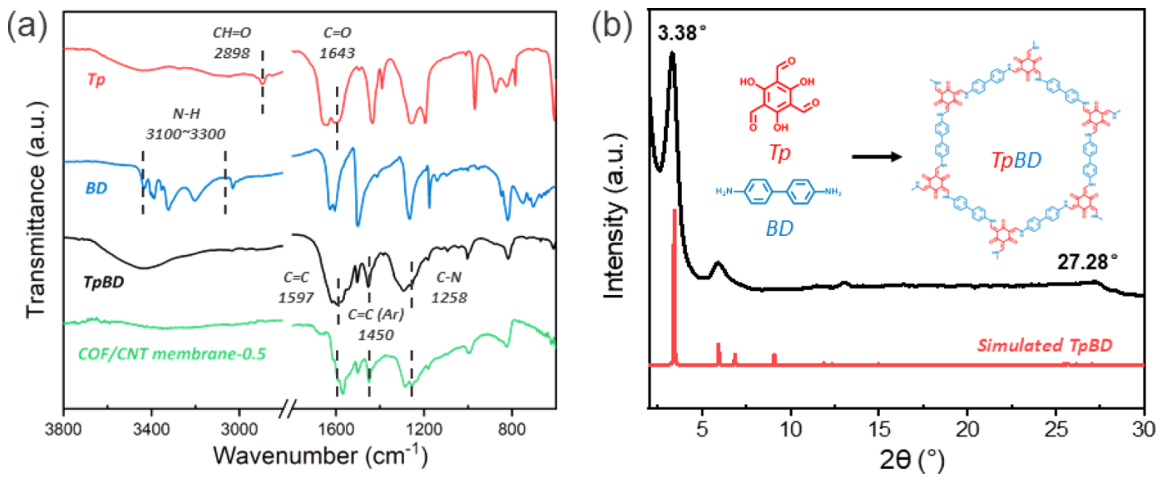

Figure 2. (a) FTIR spectra of Tp, BD, TpBD particulates, and COF/CNT membranes. (b) PXRD pattern and simulated PXRD pattern of TpBD (insets show the chemical construction of Tp, BD, and TpBD).

https://doi.org/10.1021/acs.iecr.1c01254
Ind. Eng. Chem. Res. 2021, 60, 8687−8695

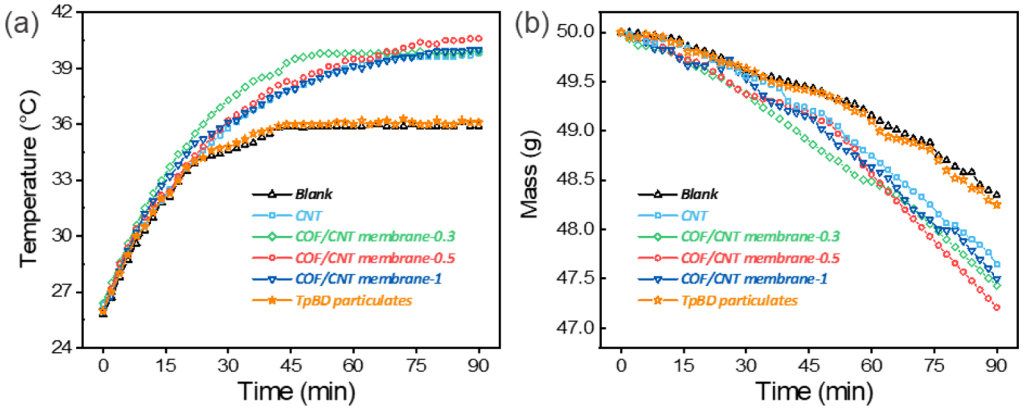

Figure 3. Changes of (a) temperature and (b) mass of dye solutions during photocatalytic degradation of MB17 with various photocatalysts.

COF/CNT membranes, the temperature and mass of the dye solution changed significantly with the increasing of photocatalysis time. As shown in Figure 3a,b, after simulated sunlight irradiation for 90 min, the blank dye solution (without addition of any photocatalysts) and the TpBD-particulate-added solution sample had similar temperature and mass changes. The temperature was increased from 25 to 36 °C and the mass was decreased from 50 to ~48.3 g. In contrast, the CNT membranes and COF/CNT membranes exhibited a stronger photothermal effect. Taking COF/CNT membrane-0.5 as an example, after irradiation with simulated sunlight for 90 min, the temperature of the system was increased from 25 to 40.6 °C, which was 73.3% higher than that of the blank solution. The weight loss of the system was 2.79 g, which was 64.1% higher than that of the blank solution. After adding COF/CNT membranes, the solution system absorbed more light, thus introducing more energy into the photocatalysis system. The temperature was increased substantially and more water was evaporated. In the photothermal effect comparison, COF/CNT membranes performed slightly better than the CNT membranes. Due to the strong surface hydrophobicity, the CNT membranes floated above the water surface during the photocatalysis process, reducing the energy conversion efficiency. As shown in Figure S1, after synthesis of the COF photocatalytic layer, the contact angle of COF/CNT membranes was dropped from the initial 126° to lower than 54°. The hydrophilicity of the CNT membranes was greatly improved, and COF/CNT membranes could be fully immersed below the water surface during the photocatalytic process. In photocatalysis, higher temperature was beneficial to the improvement of catalyst activity and the migration of active free radicals, which could significantly improves the degradation performance.[42] Moreover, the solution was concentrated with increasing temperature, which facilitated the adsorption of MB17 on the surface of the membranes, and improved photocatalytic efficiency.

In the photocatalytic degradation process, due to the excellent adsorption of the CNT membranes and COFs, contaminants absorbed on the surface became a non-negligible factor. In addition, the process of adsorption was dynamically equilibrious and the adsorption of photocatalysts was variable with the concentration of solutions. Therefore, dyes in solutions and membranes should be taken into consideration when calculating degradation capacity. The CNT membrane and COF/CNT membrane-0.5 were immersed in MB17 solutions with different concentrations (20−120 mg/L). After 12 h in the dark, equilibrium adsorption curves at 25 °C were obtained (Figure S2). After reaching equilibrium, the functional curve between equilibrium adsorption capacities and equilibrium solution concentrations kept good linear relation in the range of 0 to 100 mg/L, and the adsorption capacity of CNT membranes was similar to that of COF/CNT membranes.

In order to distinguish the influence of adsorption from photocatalysis, both CNT membranes and COF/CNT membranes were subjected to equilibrium adsorption for 12 h in the dark before photocatalysis. According to the equilibrium adsorption curves, about 7.5 mg dyes were adsorbed on the CNT membranes and COF/CNT membranes. As shown in Figure 4, COF/CNT membranes showed

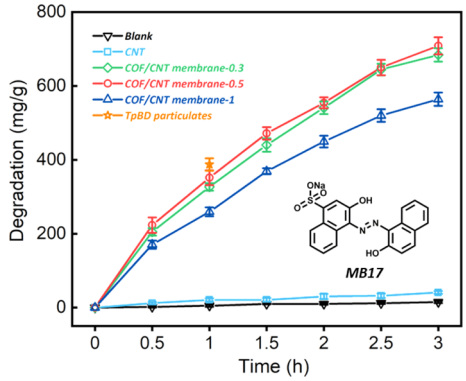

Figure 4. Photocatalytic degradation of MB17 by CNT membranes, COF/CNT membranes, and TpBD particulates (inset shows the chemical structure of MB17). "Blank" indicates no photocatalysts were added into the dye solution.

significant photocatalytic degradation performance toward MB17 solution under simulated sunlight. Due to the large adsorption capacity of membranes, the dye adsorbed in membranes was even more than that in equilibrious solutions. Therefore, the unit degradation amount (the mass of dye degraded by unit photocatalyst, mg/g) including that in adsorptions and solutions was used as a parameter to indicate degradation performance instead of the frequently used degradation percentage.

After irradiation for 3 h, the concentration of the blank dye solution and the CNT-membrane added solution remained almost unchanged, which proved that MB17 was stable without catalysts and the degradation effect of the CNT

https://doi.org/10.1021/acs.iecr.1c01254
Ind. Eng. Chem. Res. 2021, 60, 8687−8695

membranes was negligible. The concentration of MB17 changed significantly when using COF/CNT membranes as the photocatalyst. COF/CNT membrane-0.3 and COF/CNT membrane-0.5 exhibited similar photocatalytic degradation capacity. When the monomer concentration was increased to 1 mmol, the photocatalytic efficiency was decreased. As we discussed above, due to excess monomers, the COF grew into patches on the surface of the membrane, and the interspace of CNTs was filled up. The discrete growth was unfavorable for the migration of photo-generated electrons, and led to rapid recombination of hole−electron pairs and photocatalytic degradation capacity reduction of COF/CNT membranes. Moreover, the COF patches reduced the contacting surface area with dyes, part of the photocatalyst was inactive, which was not beneficial to the degradation processes.[43]

Compared with the case of TpBD particulates,[38] COF/CNT membrane-0.5 showed similar degradation capacity after irradiation for 1 h. In the solution system, a better dispersion of photocatalysts resulted in a higher migration efficiency of the photoelectrons, which accelerated the photocatalytic degradation. TpBD particulates were homogeneously dispersed in the dye solution under stirring, thus having more chances to contact dye molecules and consequently exhibiting better degradation. However, in the process of long-term use, particulates are liable to agglomerate, causing a huge loss to photocatalysis efficiency. Meanwhile, it was also hard to recover the particulates from solutions, usually requiring additional processes in engineering applications. Photocatalysts in the form of membranes with large lateral sizes, maximizing the illumination area, ensured the utilization of the sunlight. Membranes can be easily put into solutions to initiate the photocatalysis and taken out from the solution for recycles and reuses, which is highly desired in real applications. Moreover, membrane form photocatalysts are more convenient to be modified and programmed into industrial processes. Fixing photocatalysts on substrates completely eliminated the possibility of agglomeration, which was a prevalent problem for powder form photocatalysts. Combining with the advantages of substrates would also deepen the practical significance of photocatalysis. All the merits mentioned above greatly improved the handleability of the membrane form photocatalysts. As shown in Table S2, compared to other photocatalysts (organic, inorganic, or doped), COF/CNT membranes show a better photocatalytic performance.

Ultraviolet light only accounts 8% of the total sunlight.[12] Therefore, a wider absorption edge and an appropriate band gap are important factors for the photocatalysts to utilize natural light. As shown in Figure S3a, diffuse reflectance spectrophotometry (DRS) was used to test the absorption edge and band gap of TpBD (2.19 eV).The absorption edge of TpBD is close to 600 nm, while that of the traditional photocatalyst TiO_2 was only 320 nm.[42] The improvement of the absorption edge of TpBD is expected to greatly increase the utilization efficiency of natural light. The semiconductor type of TpBD can be determined by the M−S analysis, and the energy band structure information such as flat band potential and conduction band potential can be obtained after calculation. As shown in Figure S3b, the slope of the M−S curve was positive, indicating that TpBD was an n-type semiconductor. The flat band potential of TpBD was −1.21 V (vs Ag/AgCl) and the conduction band potential of TpBD was −0.8 V (vs RHE). Combining the band gap obtained by the DRS of 2.19 eV, the corresponding valence band potential of TpBD was calculated to be 1.39 V (*vs* RHE). Calculation details are shown in Supporting Information Section S5.

Scavengers were used to study the main active radicals of COF/CNT membranes during photocatalytic degradation. After natural light irradiation, photoelectrons were generated and migrated to the surface of the catalyst to combine oxygen-containing compounds in the aquatic milieu. Then, the generated oxygen-containing free radicals degraded the dyes through redox reactions. During the photocatalytic degradation of TpBD, three redox free radicals, $^{\bullet}O_2^-$, $^{\bullet}OH$, and h^+ were generated. Therefore, BQ, *t*-BuOH, and EDTA-2Na were used as scavengers to capture the active free radicals generated during the degradation processes (for $^{\bullet}O_2^-$, $^{\bullet}OH$, and h^+, respectively). The major radical in the photocatalytic process was determined by comparing the recessions of degradation capacity with different scavengers.[44] As shown in Figure 5, the

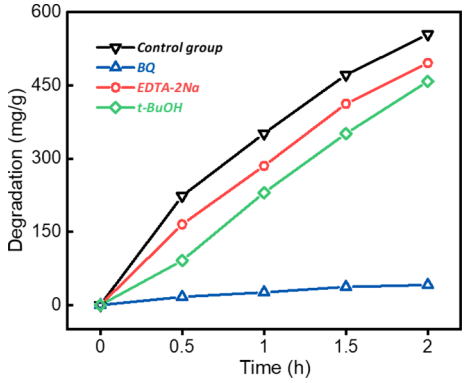

Figure 5. Degradation performance of MB17 with different scavengers.

degradation capacity of COF/CNT membrane-0.5 was greatly reduced by adding BQ. After irradiation for 2 h, the photocatalytic degradation capacity was reduced by 92.6% compared with the control group. In contrast, the impact of adding *t*-BuOH and EDTA-2Na was relatively weak, with decrease of only 17.4 and 10.6%, respectively. Therefore, in photocatalytic degradation of MB17 by COF/CNT membranes, $^{\bullet}O_2^-$ was the most active radical, while $^{\bullet}OH$ and h^+ were functioning as auxiliary agents.

3.3. Durability and Reusability. We then tested the mechanical properties of the CNT membranes and COF/CNT membranes. The initial CNT membranes were soft and ductile. At 25% tensile strain, the membranes fractured and exhibited a low stress of ∼170 MPa. Nevertheless, the pure CNT membranes were not stable to maintain the original structure in actual use, and prone to breakage.[45] As shown in the inset of Figure 6a, the CNT membranes were broken into pieces under agitation by a magnetic bar for 1 h. In contrast, the mechanical strength of CNT membranes was greatly enhanced after growing of COF layers, and the COF/CNT membranes maintained their original structural integrity after stirring for 1 h. As the monomer concentration increased, the tensile stress of COF/CNT membranes increased significantly, but the ductility decreased. When the concentration was 0.5 mmol, the tensile stress was 230 MPa, similar to that of COF/CNT membrane-1, which was 35% higher than that of the base membranes. Meanwhile, the tensile strain was about 16%, similar to that of COF/CNT membrane-0.3. With the appropriate monomer concentration, COF grew uniformly

https://doi.org/10.1021/acs.iecr.1c01254
Ind. Eng. Chem. Res. 2021, 60, 8687−8695

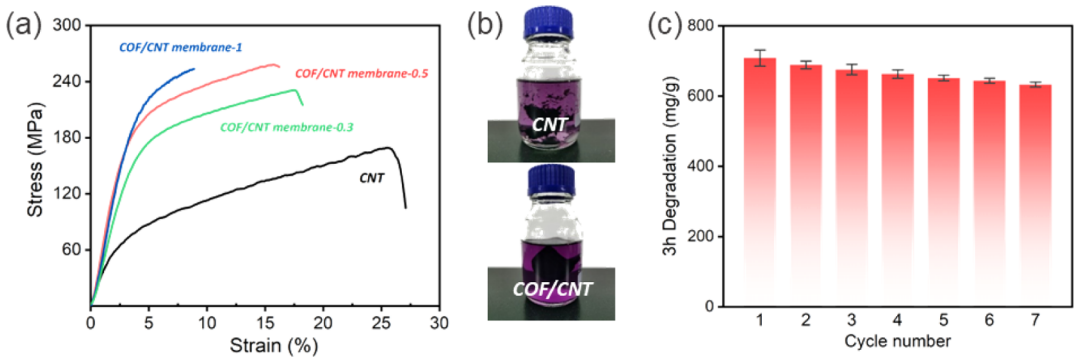

Figure 6. (a) Stress−strain curve of COF/CNT membranes, (b) appearance of membranes after 200 rpm stirring for 1 h, and (c) reusability of COF/CNT membrane-0.5 in photocatalytic degradation.

along the CNTs, which improved the mechanical strength of COF/CNT membranes at affordable expense of ductility. COF/CNT membrane-0.5 exhibited good mechanical properties and maintained its original structure during operation (Figure 6b).

Due to the mechanical robustness and the photocatalytic stability of nonmetal semiconductors, COF/CNT membranes showed excellent reusability in the photocatalytic degradation of MB17. As shown in Figure 6c, COF/CNT membranes retained high degradation performance after seven cycles of test. In the seventh test, degradation of MB17 reached 632.8 mg/g in 3 h. Compared with 708.2 mg/g at the first test, only 10.6% efficiency was lost, which can be attributed to the detachment of the COF coating caused by stirring and photocorrosion (Figure S4). Photocatalysts in the form of membranes effectively inhibited the aggregation of catalysts in the aquatic milieu, as well as improved the durability and reusability of photocatalysts. Moreover, COF/CNT membranes did not require cleaning and regeneration after usage, which made the operation process more convenient and efficient.

4. CONCLUSIONS

In this work, COFs are grown on the CNT membranes successfully and the fabricated COF/CNT membranes exhibit superior photocatalytic activity. By utilizing the large surface area and photothermal effect of the CNT membranes, the photocatalytic activity of COF-based composite membranes can be improved to match that of pure TpBD particulates. Combining photocatalysts with substrates not only eliminates the powder agglomeration and ensures the utilization of the sunlight, but also simplifies the recovery process and greatly promotes the handleability in real applications on a large scale. Benefiting from the low band gap energy of the TpBD, COF/CNT membranes can use natural light to efficiently degrade synthetic dyes. We also demonstrate that the generated $^{\bullet}O_2^-$ is the most active radical during the degradation processes. Meanwhile, the mechanical strength of the CNT membranes is greatly improved by TpBD growth. The total degradation capacity for COF/CNT membranes can reach 708.2 mg/g, and the membranes can be reused seven times without a significant decline in degradation capacity. This work combines the advantages of both CNTs and COFs and provides a new strategy to prepare photocatalytic membranes, which can be easily reused in dye degradation.

■ ASSOCIATED CONTENT

Supporting Information

The Supporting Information is available free of charge at https://pubs.acs.org/doi/10.1021/acs.iecr.1c01254.

Mass changes; water contact angles; equilibrium adsorption curves; degradation performance comparison; energy band structures; and durability and reusability (PDF)

■ AUTHOR INFORMATION

Corresponding Authors

Sen Xiong − *State Key Laboratory of Materials-Oriented Chemical Engineering, and College of Chemical Engineering, Nanjing Tech University, Nanjing 211816, Jiangsu, P. R. China*; Phone: +86-25-83172247; Email: xiongsenhg@njtech.edu.cn; Fax: +86-25-83172292

Yong Wang − *State Key Laboratory of Materials-Oriented Chemical Engineering, and College of Chemical Engineering, Nanjing Tech University, Nanjing 211816, Jiangsu, P. R. China*; orcid.org/0000-0002-8653-514X; Email: yongwang@njtech.edu.cn

Authors

Hongbo Xue − *State Key Laboratory of Materials-Oriented Chemical Engineering, and College of Chemical Engineering, Nanjing Tech University, Nanjing 211816, Jiangsu, P. R. China*

Zhijie Bi − *State Key Laboratory of Materials-Oriented Chemical Engineering, and College of Chemical Engineering, Nanjing Tech University, Nanjing 211816, Jiangsu, P. R. China*

Jiayu Cheng − *State Key Laboratory of Materials-Oriented Chemical Engineering, and College of Chemical Engineering, Nanjing Tech University, Nanjing 211816, Jiangsu, P. R. China*

Complete contact information is available at: https://pubs.acs.org/10.1021/acs.iecr.1c01254

Notes

The authors declare no competing financial interest.

■ ACKNOWLEDGMENTS

We gratefully acknowledge financial support from the National Key Research and Development Program of China (2018YFE0203502), Jiangsu Natural Science Foundation (BK20190677), National Natural Science Foundation of

China (21908096), and Program of Excellent Innovation Teams of Jiangsu Higher Education Institutions.

REFERENCES

(1) Mondal, S. Methods of Dye Removal from Dye House Effluent-An Overview. *Environ. Eng. Sci.* **2008**, *25*, 383−396.
(2) Singh, T. S. A.; Ramesh, S. T. New Trends in Electrocoagulation for the Removal of Dyes from Wastewater: A Review. *Environ. Eng. Sci.* **2013**, *30*, 333−349.
(3) Solís, M.; Solís, A.; Pérez, H. I.; Manjarrez, N.; Flores, M. Microbial Decolouration of Azo Dyes: A Review. *Process Biochem.* **2012**, *47*, 1723−1748.
(4) Yaseen, D. A.; Scholz, M. Textile Dye Wastewater Characteristics and Constituents of Synthetic Effluents: A Critical Review. *Int. J. Environ. Sci. Technol.* **2019**, *16*, 1193−1226.
(5) Fu, Y.; Viraraghavan, T. Fungal Decolorization of Dye Wastewaters: A Review. *Bioresour. Technol.* **2001**, *79*, 251−262.
(6) Zhou, Y.; Lu, J.; Zhou, Y.; Liu, Y. Recent Advances for Dyes Removal Using Novel Adsorbents: A Review. *Environ. Pollut.* **2019**, *252*, 352−365.
(7) Saratale, R. G.; Saratale, G. D.; Chang, J. S.; Govindwar, S. P. Bacterial Decolorization and Degradation of Azo Dyes: A Review. *J. Taiwan Inst. Chem. Eng.* **2011**, *42*, 138−157.
(8) Rovira, J.; Domingo, J. L. Human Health Risks Due to Exposure to Inorganic and Organic Chemicals from Textiles: A Review. *Environ. Res.* **2019**, *168*, 62−69.
(9) Robinson, T.; McMullan, G.; Marchant, R.; Nigam, P. Remediation of Dyes in Textile Effluent: A Critical Review on Current Treatment Technologies with a Proposed Alternative. *Bioresour. Technol.* **2001**, *77*, 247−255.
(10) Pang, Y. L.; Abdullah, A. Z. Current Status of Textile Industry Wastewater Management and Research Progress in Malaysia: A Review. *Clean: Soil, Air, Water* **2013**, *41*, 751−764.
(11) Xu, C.; Ravi Anusuyadevi, P.; Aymonier, C.; Luque, R.; Marre, S. Nanostructured Materials for Photocatalysis. *Chem. Soc. Rev.* **2019**, *48*, 3868−3902.
(12) Zhou, Q. Q.; Zou, Y. Q.; Lu, L. Q.; Xiao, W. J. Visible-Light-Induced Organic Photochemical Reactions through Energy-Transfer Pathways. *Angew. Chem. Int. Ed.* **2019**, *58*, 1586−1604.
(13) Likodimos, V. Photonic Crystal-Assisted Visible Light Activated TiO_2 Photocatalysis. *Appl. Catal., B* **2018**, *230*, 269−303.
(14) Jiao, L.; Wang, Y.; Jiang, H.; Xu, Q. Metal-Organic Frameworks as Platforms for Catalytic Applications. *Adv. Mater.* **2018**, *30*, 1703663.
(15) Reddy, K. R.; Reddy, C. V.; Nadagouda, M. N.; Shetti, N. P.; Jaesool, S.; Aminabhavi, T. M. Polymeric Graphitic Carbon Nitride (g-C_3N_4)-Based Semiconducting Nanostructured Materials: Synthesis Methods, Properties and Photocatalytic Applications. *J. Environ. Manage.* **2019**, *238*, 25−40.
(16) Pei, C.-Y.; Chen, Y.-G.; Wang, L.; Chen, W.; Huang, G.-B. Step-Scheme WO_3/$CdIn_2S_4$ Hybrid System with High Visible Light Activity for Tetracycline Hydrochloride Photodegradation. *Appl. Surf. Sci.* **2021**, *535*, 147682.
(17) Fang, M.-M.; Shao, J.-X.; Huang, X.-G.; Wang, J.-Y.; Chen, W. Direct Z-Scheme $CdFe_2O_4$/g-C_3N_4 Hybrid Photocatalysts for Highly Efficient Ceftiofur Sodium Photodegradation. *J. Mater. Sci. Technol.* **2020**, *56*, 133−142.
(18) Mehrjouei, M.; Müller, S.; Möller, D. A Review on Photocatalytic Ozonation Used for the Treatment of Water and Wastewater. *Chem. Eng. J.* **2015**, *263*, 209−219.
(19) Byrne, C.; Subramanian, G.; Pillai, S. C. Recent Advances in Photocatalysis for Environmental Applications. *J. Environ. Chem. Eng.* **2018**, *6*, 3531−3555.
(20) Geng, K.; He, T.; Liu, R.; Dalapati, S.; Tan, K. T.; Li, Z.; Tao, S.; Gong, Y.; Jiang, Q.; Jiang, D. Covalent Organic Frameworks: Design, Synthesis, and Functions. *Chem. Rev.* **2020**, *120*, 8814−8933.
(21) Chen, X.; Geng, K.; Liu, R.; Tan, K. T.; Gong, Y.; Li, Z.; Tao, S.; Jiang, Q.; Jiang, D. Covalent Organic Frameworks: Chemical Approaches to Designer Structures and Built-In Functions. *Angew. Chem. Int. Ed.* **2020**, *59*, 5050−5091.
(22) Afshari, M.; Dinari, M.; Zargoosh, K.; Moradi, H. Novel Triazine-Based Covalent Organic Framework as a Superadsorbent for the Removal of Mercury(Ii) from Aqueous Solutions. *Ind. Eng. Chem. Res.* **2020**, *59*, 9116−9126.
(23) Mokhtari, N.; Khataei, M. M.; Dinari, M.; Hosseini Monjezi, B.; Yamini, Y. Imine-Based Covalent Triazine Framework: Synthesis, Characterization, and Evaluation Its Adsorption. *Mater. Lett.* **2020**, *263*, 127221.
(24) Babu, H. V.; Bai, M. G. M.; Rajeswara Rao, M. Functional π-Conjugated Two-Dimensional Covalent Organic Frameworks. *ACS Appl. Mater. Interfaces* **2019**, *11*, 11029−11060.
(25) Liang, R.-R.; Zhao, X. Heteropore Covalent Organic Frameworks: A New Class of Porous Organic Polymers with Well-Ordered Hierarchical Porosities. *Org. Chem. Front.* **2018**, *5*, 3341−3356.
(26) Iwase, A.; Yoshino, S.; Takayama, T.; Ng, Y. H.; Amal, R.; Kudo, A. Water Splitting and CO_2 Reduction under Visible Light Irradiation Using Z-Scheme Systems Consisting of Metal Sulfides, CoO_x-Loaded $BiVO_4$, and a Reduced Graphene Oxide Electron Mediator. *J. Am. Chem. Soc.* **2016**, *138*, 10260−10264.
(27) Pachfule, P.; Acharjya, A.; Roeser, J.; Langenhahn, T.; Schwarze, M.; Schomäcker, R.; Thomas, A.; Schmidt, J. Diacetylene Functionalized Covalent Organic Framework (COF) for Photocatalytic Hydrogen Generation. *J. Am. Chem. Soc.* **2018**, *140*, 1423−1427.
(28) Fu, Y.; Zhu, X.; Huang, L.; Zhang, X.; Zhang, F.; Zhu, W. Azine-Based Covalent Organic Frameworks as Metal-Free Visible Light Photocatalysts for CO_2 Reduction with H_2O. *Appl. Catal., B* **2018**, *239*, 46−51.
(29) Bhadra, M.; Kandambeth, S.; Sahoo, M. K.; Addicoat, M.; Balaraman, E.; Banerjee, R. Triazine Functionalized Porous Covalent Organic Framework for Photo-Organocatalytic E-Z Isomerization of Olefins. *J. Am. Chem. Soc.* **2019**, *141*, 6152−6156.
(30) Liu, T.; Hu, X.; Wang, Y.; Meng, L.; Zhou, Y.; Zhang, J.; Chen, M.; Zhang, X. Triazine-Based Covalent Organic Frameworks for Photodynamic Inactivation of Bacteria as Type-Ii Photosensitizers. *J. Photochem. Photobiol., B* **2017**, *175*, 156−162.
(31) Zhang, Y.; Hu, Y.; Zhao, J.; Park, E.; Jin, Y.; Liu, Q.; Zhang, W. Covalent Organic Framework-Supported Fe-TiO_2 Nanoparticles as Ambient-Light-Active Photocatalysts. *J. Mater. Chem. A* **2019**, *7*, 16364−16371.
(32) Yang, X.; Wan, Y.; Zheng, Y.; He, F.; Yu, Z.; Huang, J.; Wang, H.; Ok, Y. S.; Jiang, Y.; Gao, B. Surface Functional Groups of Carbon-Based Adsorbents and Their Roles in the Removal of Heavy Metals from Aqueous Solutions: A Critical Review. *Chem. Eng. J.* **2019**, *366*, 608−621.
(33) Jiang, D.; Ma, W.; Xiao, P.; Shao, L.; Li, D.; Chen, M. Enhanced Photocatalytic Activity of Graphitic Carbon Nitride/Carbon Nanotube/Bi_2WO_6 Ternary Z-Scheme Heterojunction with Carbon Nanotube as Efficient Electron Mediator. *J. Colloid Interface Sci.* **2018**, *512*, 693−700.
(34) Li, Y.; Cui, X.; Zhao, M.; Xu, Y.; Chen, L.; Cao, Z.; Yang, S.; Wang, Y. Facile Preparation of a Robust Porous Photothermal Membrane with Antibacterial Activity for Efficient Solar-Driven Interfacial Water Evaporation. *J. Mater. Chem. A* **2019**, *7*, 704−710.
(35) Wang, J.; Li, B.; Yang, D.; Lv, H.; Zhang, C. Preparation of an Octahedral Ptni/Cnt Catalyst and Its Application in High Durability Pemfc Cathodes. *RSC Adv.* **2018**, *8*, 18381−18387.
(36) Dai, B.; Fang, J.; Yu, Y.; Sun, M.; Huang, H.; Lu, C.; Kou, J.; Zhao, Y.; Xu, Z. Construction of Infrared-Light-Responsive Photo-induced Carriers Driver for Enhanced Photocatalytic Hydrogen Evolution. *Adv. Mater.* **2020**, *32*, No. e1906361.
(37) Shi, L.; Shi, Y.; Zhang, C.; Zhuo, S.; Wang, W.; Li, R.; Wang, P. An Integrated Photocatalytic and Photothermal Process for Solar-Driven Efficient Purification of Complex Contaminated Water. *Energy Technol.* **2020**, *8*, 2000456.

https://doi.org/10.1021/acs.iecr.1c01254
Ind. Eng. Chem. Res. 2021, 60, 8687−8695

(38) Xue, H.; Xiong, S.; Mi, K.; Wang, Y. Visible-Light Degradation of Azo Dyes by Imine-Linked Covalent Organic Frameworks. *Green Energy Environ.* **2021**, DOI: 10.1016/j.gee.2020.09.010.
(39) Labanda, J.; Sabaté, J.; Llorens, J. Modeling of the Dynamic Adsorption of an Anionic Dye through Ion-Exchange Membrane Adsorber. *J. Membr. Sci.* **2009**, *340*, 234−240.
(40) Biswal, B. P.; Chandra, S.; Kandambeth, S.; Lukose, B.; Heine, T.; Banerjee, R. Mechanochemical Synthesis of Chemically Stable Isoreticular Covalent Organic Frameworks. *J. Am. Chem. Soc.* **2013**, *135*, 5328−5331.
(41) Chandra, S.; Kandambeth, S.; Biswal, B. P.; Lukose, B.; Kunjir, S. M.; Chaudhary, M.; Babarao, R.; Heine, T.; Banerjee, R. Chemically Stable Multilayered Covalent Organic Nanosheets from Covalent Organic Frameworks Via Mechanical Delamination. *J. Am. Chem. Soc.* **2013**, *135*, 17853−17861.
(42) Nakata, K.; Fujishima, A. TiO_2 photocatalysis: Design and applications. *J. Photochem. Photobiol., C* **2012**, *13*, 169−189.
(43) You, J.; Guo, Y.; Guo, R.; Liu, X. A Review of Visible Light-Active Photocatalysts for Water Disinfection: Features and Prospects. *Chem. Eng. J.* **2019**, *373*, 624−641.
(44) Lv, H.; Zhao, X.; Niu, H.; He, S.; Tang, Z.; Wu, F.; Giesy, J. P. Ball Milling Synthesis of Covalent Organic Framework as a Highly Active Photocatalyst for Degradation of Organic Contaminants. *J. Hazard. Mater.* **2019**, *369*, 494−502.
(45) Shaari, N.; Kamarudin, S. K. Recent advances in additive-enhanced polymer electrolyte membrane properties in fuel cell applications: An overview. *Int. J. Energy Res.* **2019**, *43*, 2756−2794.

https://doi.org/10.1021/acs.iecr.1c01254
Ind. Eng. Chem. Res. 2021, 60, 8687−8695